 Open access • Book Chapter • DOI:10.1007/BFB0018284

## Methods of emittance measurement — Source link

Kirk T. McDonald, D.P. Russell

**Institutions:** Princeton University

**Published on:** 01 Jan 1989 - Lecture Notes in Physics (Springer, Berlin, Heidelberg)

**Topics:** Accelerator Test Facility, Thermal emittance, Laser beam quality and Phase space

Related papers:

- [Nonintercepting emittance monitor](#)
- [Study for Emittance Measurements in a High-Current Multibeamlet Beam](#)
- [Reducing longitudinal emittance growth in RFQ accelerators](#)
- [Third-generation electron beams at the accelerator test facility for JLC](#)
- [Emittance Measurement of Axisymmetric High-Current Electron Beam Confined by a Longitudinal Magnetic Field : Instrumentation, Measurement, and Fabrication Technology](#)

Share this paper:    

View more about this paper here: <https://typeset.io/papers/methods-of-emittance-measurement-yqegsb5cue>

# Methods of Emittance Measurement

K.T. McDonald and D.P. Russell

*Joseph Henry Laboratories, Princeton University, Princeton, NJ 08544*

(Oct. 20, 1988)

## Abstract

We discuss experimental techniques for measurement of the density of beam particles in both the transverse and longitudinal phase space. The second moments of a two-dimensional density in conjugate coordinates are combined to form the emittance, which remains invariant under idealized beam transport. Four different methods of emittance measurement are presented, as will be implemented at the Brookhaven Accelerator Test Facility.

## 1 Introduction

There is an ever-increasing number of uses for high-quality charged-particle beams, with such diverse applications as nuclear and particle-physics experiments, electron microscopy, and medical diagnosis and treatment. It is important to have a measure of the quality of such beams in terms of their ability to be transported over long distances, to be focused into a small space with a minimum of divergence, and to form high-resolution images. The same issues arise in the use of laser beams, though the language describing analogous optical and particle beam properties is not the same. Also, while the fundamental limits on optical beam quality are set by the laws of quantum mechanics, it will be seen that the quality of a particle beam is limited by statistical mechanics.

A beam of particles can be characterized in detail by its density in the six-dimensional *phase space*,  $(x, p_x, y, p_y, z, p_z)$ , where  $\mathbf{p}$  is the canonical momentum. The utility of a such a description derives from the discovery by Liouville [1] that the density in phase space of a system of noninteracting particles subject to a Hamiltonian (such as that of an electromagnetic field) is constant in time. Accordingly, the extent of the beam in phase space, termed its *emittance*, is also constant in time, at least under ideal conditions.

The concept of beam emittance is a most useful one, but is often abused in practice. There is a number of closely related but distinct quantities all referred to as “emittance”. The conditions under which these quantities are conserved should be understood, and the degree to which these conditions are satisfied in a given application should be considered when quoting an emittance. We will use the terminology employed by LeJeune and Aubert. [2].

In practice the six-dimensional description is usually split into three two-dimensional subspaces,  $(x, p_x)$ ,  $(y, p_y)$ , and  $(z, p_z)$ , where  $z$  is taken as the average direction, or *optic axis*, of the beam. The emittance is defined in terms of the area occupied by the beam in these two-dimensional spaces. If the area occupied by the beam in the  $(x, p_x)$  plane is  $\Gamma^x$ , then the *normalized* or *invariant emittance* is defined as

$$\epsilon_n^x \equiv \Gamma^x / \pi m_0 c,$$

where  $m_0$  is the electron rest mass and  $c$  is the speed of light.

In practice it is not the transverse momenta of beam particles that are usually measured, but rather the gradients of the trajectories in the  $x$ - $z$  and  $y$ - $z$  planes. Hence another frequently-used definition is obtained by replacing the variable  $p_x$  with  $x' = dx/dz = v_x/v_z$ . The space of  $(x, x')$  is called the *trace space*. If the area occupied by the beam in trace space is  $A^x$ , then the *geometric emittance* is defined as

$$\epsilon^x \equiv A^x/\pi. \quad (1)$$

The term ‘‘emittance’’ used without a modifying adjective often refers to the quantity defined by Eq. (1), and this will be our convention. From the definitions it is seen that  $\epsilon_n^x = \gamma\beta_z\epsilon^x$ , where  $\beta_z = v_z/c$  and  $\gamma = 1/\sqrt{1-\beta^2}$ . Similar definitions apply to the  $y$  and  $z$  spaces. The normalized and geometric emittance have units of distance-times-angle, such as m-rad or mm-mrad. In fact, very often in characterizing a beam the slope  $x'$  is replaced by the angle  $\theta_x$ . This is valid in the paraxial (Gaussian-optics) approximation, for which  $x' = \tan\theta_x \approx \theta_x$ . The ‘‘paraxial-ray formalism’’ is an analytical approach to beam dynamics which assumes that the particles travel very near a central trajectory, and only linear transverse variations of the electric and magnetic fields are considered.

These definitions, in referring to the area occupied by a beam, assume a hard-edged distribution. However, they are easily generalized to more realistic distributions with no well-defined cutoff. Often the density distribution,  $\rho$ , of a beam can be adequately characterized by a quadratic function of the trace- (or phase-) space variables:

$$\rho(x, x') = \rho(\mathbf{x}^T \sigma^{-1} \mathbf{x}),$$

where  $\mathbf{x}$  is the trace space vector  $(x, x')$  and  $\sigma$  is the symmetric beam matrix

$$\sigma = \begin{pmatrix} \sigma_{11} & \sigma_{12} \\ \sigma_{12} & \sigma_{22} \end{pmatrix}. \quad (2)$$

Often the density function  $\rho$  is a Gaussian:

$$\rho(x, x') = N \exp \left[ \frac{-(\sigma_{22}x^2 - 2\sigma_{12}xx' + \sigma_{11}x'^2)}{2 \det \sigma} \right]. \quad (3)$$

The matrix elements are just the second moments of the distribution, *i.e.*,  $\sqrt{\sigma_{11}}$  is just the standard deviation of the distribution in  $x$  obtained by integrating  $\rho$  over  $x'$ . In this case the emittance is often defined as

$$\epsilon^x \equiv \sqrt{\det \sigma} = \sqrt{\sigma_{11}\sigma_{22} - \sigma_{12}^2}.$$

This corresponds to  $1/\pi$  times the area occupied by the elliptical contour which contains 39.3% of the beam defined by Eq. (3).

It should be noted in passing that one sometimes sees a beam characterized by the *Twiss parameters*. These are just the beam-matrix elements normalized by the emittance and defined as follows:  $\alpha \equiv -\sigma_{12}/\epsilon$ ,  $\beta \equiv \sigma_{11}/\epsilon$ , and  $\gamma \equiv \sigma_{22}/\epsilon$ . In terms of the Twiss parameters the equation of the beam ellipse may be written

$$\gamma x^2 + 2\alpha x x' + \beta x'^2 = \epsilon,$$

and  $\beta\gamma - \alpha^2 = 1$ .

One other definition of emittance has been developed by Lapostolle [3] which is applicable to general beam distributions without an easily defined shape. This is the *r.m.s. emittance*,  $\bar{\epsilon}$ , the definition of which is based on the concept of the “equivalent perfect beam”. This is an imaginary beam which has a uniform distribution within a hard-edged elliptical contour and which has the same second moments and total intensity as the given beam. The r.m.s. emittance is given as  $1/\pi$  times the area in trace space of the equivalent perfect beam. This may be shown to be

$$\bar{\epsilon} = 4 \left[ \langle x^2 \rangle \langle x'^2 \rangle - \langle xx' \rangle^2 \right]^{1/2},$$

and this is taken as the definition of the r.m.s. emittance of a beam distribution in general. We see that for a Gaussian distribution  $\bar{\epsilon} = 4\epsilon$ , corresponding to a contour containing 86.5% of the beam.

The validity of such measures depends on several assumptions that will be noted here but not examined closely:

- The particles do not interact with one another. Coulomb interactions lead to “space-charge” growth of the emittance.
- The beam transport does not couple the various two-dimensional projections of the six-dimensional phase space. Certain beamline elements such as sextupole magnets and rf kickers in fact provide coupling between the subspaces.
- Higher moments than the second are not needed to characterize the density in phase space. This is true so long as the effects of the beamline elements are accurately described by linear transformations (Gaussian optics). Nonlinear elements lead to distortions of the phase volume that do not violate Liouville’s theorem but render a second-moment description inadequate. In fact the increase in the r.m.s. emittance is often a good measure of the nonlinearity of a transport system.
- There are situations in which the normalized emittance is conserved but the geometric emittance is not, and *vice versa*. Recall that for a particle of charge  $q$  in a vector potential  $\mathbf{A}$ , the canonical momentum is given by  $\mathbf{p} = m_0c\gamma\vec{\beta} + q\mathbf{A}/c$ . Hence  $x$  and  $x'$  are canonically conjugate variables (resulting in the conservation of geometric emittance) only if (a) the transverse components of the vector potential,  $A_x$  and  $A_y$ , are zero and (b) the beam energy,  $\gamma$ , remains constant. Condition (a) is violated in many magnetic beamline elements, and condition (b) is violated during acceleration of the beam, resulting in a decrease of the geometric emittance while the invariant emittance remains the same.
- The reverse case occurs when the beam has a nonzero energy spread. Even in the absence of magnetic fields or acceleration, the achromaticity of a beam will cause the normalized emittance to increase during a simple drift (propagation through free space), while the geometric emittance is unaffected.

It is obvious that any given form of emittance is invariant only under certain very specific conditions!

## 2 Beam-Profile Monitors

The phase-space density and emittance of a beam are not measured directly. They must be inferred from beam properties which are available to laboratory measurement, such as the one- or two-dimensional profiles in the transverse position space  $(x, y)$ . A *beam-profile monitor* is a device which when placed in the beam's path converts the beam flux density as a function of position into a measurable signal. Past examples have included photosensitive materials such as film or quartz, current-measuring probes which are scanned through the beam, and apertures such as a hole or slit which are scanned through the beam upstream of a Faraday cup. The advent of silicon imaging devices such as the charge-coupled device (CCD) and the availability of digital computer technology have greatly simplified and improved the process of obtaining, storing, and analyzing two-dimensional images.

Such devices only sample the beam in  $x$  and  $y$ , integrating over any longitudinal structure. In order to extract the  $x'$  and  $y'$  distribution, the beam must be sampled under several different transport conditions or be subjected to a known spatial filtering upstream of a single profile measurement. Information about the longitudinal phase space can be obtained from a profile monitor by subjecting the beam to a transformation which couples the longitudinal coordinates to the transverse ones.

As an example, the front end of the electron beam transport line of the Brookhaven Accelerator Test Facility (ATF) is shown in Fig. 1 as an example of monitor placement in certain emittance-measurement schemes. Several types of beamline elements are shown: dipole magnets (D), quadrupoles (Q), collimating slits, and beam-profile monitors. When dipole D2 is on, the 4.5-MeV electron beam (which originates from a laser-excited photocathode in the gun) will be deflected into the transport line leading to the linac. The transverse emittance will be measured in this line. (The "pepper pot" is described below.) When D2 is turned off, the beam will enter the "z-line", where the longitudinal emittance will be measured using the profile monitor in conjunction with the rf kicker as described below.

### 2.1 A Phosphor-Screen Monitor

The profile monitors that will be used in the emittance measurements at the Accelerator Test Facility (ATF) consist of a phosphor screen (located inside the beam pipe) which is viewed via a  $45^\circ$  mirror by a CCD camera (Fig. 2). The phosphor,  $\text{Gd}_2\text{O}_2\text{S:Tb}$ , is deposited on a thin aluminum-foil substrate. It emits green light (550-nm peak wavelength) when excited by the passage of charged particles, about 1 photon per 30 eV deposited energy, and has a decay time of around 2 ms. The 4.5-MeV electron beam passes through the substrate, which is perpendicular to the optic axis of the beam, and excites the phosphor. The image is reflected out of the beamline by the mirror (in which the beam is stopped) and into the CCD camera. The image is digitized pixel-by-pixel by a video digitizer board and stored in a dedicated IBM PC-AT for subsequent analysis. During low-light-output running conditions an image intensifier (microchannel plate) will be attached to the camera, yielding sensitivity to individual beam particles.

Among the factors which must be considered when designing such a monitor are the spatial resolution of each component of the system, the light output of the beam-imaging element, the collection efficiency of the optical system, and the size and intensity of the beam

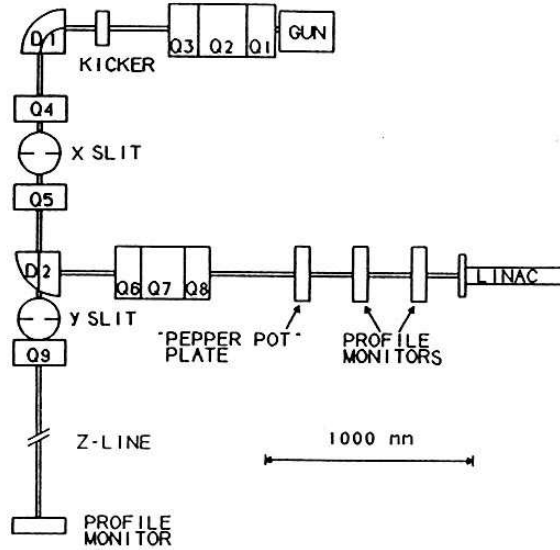


Figure 1: The front end of the electron beam transport line of the Brookhaven Accelerator Test Facility.

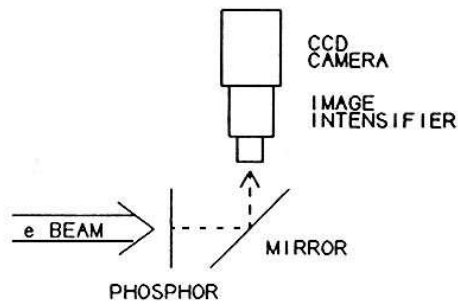


Figure 2: A phosphor-screen beam-profile monitor.

to be imaged. The ATF design should have a resolution of around  $25 \mu\text{m}$  FWHM, primarily limited by the “blooming” of the image in the  $30\text{-}\mu\text{m}$ -thick phosphor screen.

The radiation length of the phosphor screen is about 3 cm, so the r.m.s. multiple scattering angle for electrons crossing a  $30\text{-}\mu\text{m}$  screen is roughly  $1[\text{rad}]/\gamma$ . Thus the phosphor-screen alone effectively destroys the beam during the profile measurement.

## 2.2 A Transition-Radiation Monitor

A possibility for nondestructive imaging of the beam profile exists in the use of transition radiation. If the phosphor screen were removed from the monitor shown in Fig. 2, there would still be transition radiation produced as the beam enters the mirror. The rate of transition radiation integrated over optical frequencies is about  $\alpha/\pi \approx 1/500$  photon per beam particle. The direction of the transition radiation of a particle entering a metal is

along the direction of the image charge, and hence into the camera in the case of a 45° mirror as in Fig. 2. The thickness of the mirror could be only a few optical skin depths, say, 1  $\mu\text{m}$  of aluminum, leading to an r.m.s. multiple scattering angle of  $42[\text{mrad}]/\gamma$ , which may be negligible in some cases.

There is, however, a limit to the utility of transition radiation as a profile monitor set by the laws of diffraction, *i.e.*, Heisenberg's uncertainty principle.<sup>1</sup> The radiation is emitted into a cone of characteristic angle  $1/\gamma$ , and so must have originated from a region of transverse extent roughly  $\lambda\gamma$ . This region is, of course, the extent of the surface currents on the mirror whose accelerating charges actually produce the radiation. Thus the apparent size of the source of transition radiation becomes very large for highly relativistic particles and the beam profile could not be discerned. For example, 50-GeV electrons have  $\gamma = 10^5$ , so the effective spot size for optical transition radiation is about 5 cm! But for 5-Mev electrons the spot size is only 5  $\mu\text{m}$ , which is smaller than that resolvable with a phosphor screen.

### 3 Transverse-Emittance Measurement

We now consider a beam in the two-dimensional trace space  $(x, x')$  and assume the distribution is given by Eq. (3). The task is to find the emittance,  $\epsilon = \sqrt{\det \vec{\sigma}}$ . When a profile monitor intercepts the entire beam, only the spatial width at that point,  $\sqrt{\sigma_{11}}$ , is determined. However, the other matrix elements may be inferred from beam profiles taken under various transport conditions downstream of the given point if the transformation of the beam matrix between those points is understood.

If a beam has matrix  $\sigma^0$  at some point,  $z_0$ , and matrix  $\sigma^1$  at some other point,  $z_1$ , downstream, the transformation of the beam between  $z_0$  and  $z_1$  may be characterized [6] by a *transfer matrix*  $\mathbf{R}$ :

$$\mathbf{R} = \begin{pmatrix} R_{11} & R_{12} \\ R_{21} & R_{22} \end{pmatrix},$$

such that

$$\sigma^1 = \mathbf{R}\sigma^0\mathbf{R}^T,$$

where  $\mathbf{R}^T$  is the transpose of matrix  $\mathbf{R}$ . The total transfer matrix of a series of beamline components is just the product of the matrices of the individual components. Since the matrix element that we can measure at a given point is  $\sigma_{11}^1$ , we will write out the expression for this element as a function of  $\sigma^0$ :

$$\sigma_{11}^1 = R_{11}^2\sigma_{11}^0 + 2R_{11}R_{12}\sigma_{12}^0 + R_{12}^2\sigma_{22}^0. \quad (4)$$

The elements of  $\sigma^0$  can be deduced from a set of three measurements of  $\sigma_{11}$  obtained from beam conditions described by three different transfer matrices. In practice more than three independent width measurements are taken and the data subjected to least-squares analysis.

---

<sup>1</sup>Note added July 21, 2003. The conclusion of sec. 2.2 is too pessimistic because the angular distribution of transition radiation is broader than angle  $1/\gamma$ . See, for example, [4, 5]. Thanks to R. Chehab and M.S. Zolotarev for pointing this out to the authors.

### 3.1 Use of Multiple Profile Monitors

The simplest example in principle is measurement of the beam width at several locations along the beamline,  $z_i$ , separated only by drift spaces. Call the position of the first monitor  $z_0$  and the beam matrix at this point  $\sigma^0$ . The width of the beam in  $x$  at this point gives us  $\sigma_{11}^0$ . The next monitor downstream is at point  $z_1$ , where the beam matrix is  $\sigma^1$ . The transfer matrix for a drift of length  $L_1 = z_1 - z_0$  is

$$\mathbf{R}_L = \begin{pmatrix} 1 & L_1 \\ 0 & 1 \end{pmatrix}.$$

From Eq. (4) we find

$$\sigma_{11}^1 = \sigma_{11}^0 + 2L_1\sigma_{12}^0 + L_1^2\sigma_{22}^0.$$

A set of  $\sigma_{11}^i$  corresponding to several different  $L_i$  forms the system of equations from which the elements of  $\sigma^0$  are extracted. The emittance at  $z_0$  is then easily calculated as  $\epsilon = \sqrt{\sigma_{11}^0\sigma_{22}^0 - (\sigma_{12}^0)^2}$ .

This method works best if the beam comes to a waist (a point of minimum spatial extent, where  $\sigma_{12} = 0$ ), somewhere between the first and last monitors. The closer one of the monitors is to a waist, the better. If the monitor destroys or significantly perturbs the beam, the beam-width measurements will have to be performed singly with all monitors but one withdrawn from the beam path at a given time.

### 3.2 Use of Variable Quadrupole Strengths

Another way to vary the transfer matrix elements is to change the parameters of a magnetic beamline element such as a quadrupole lens.

The transfer matrix in the focusing plane for a quadrupole of magnetic-field gradient  $G$  is

$$\mathbf{R}_f = \begin{pmatrix} \cos kl & (1/k) \sin kl \\ -k \sin kl & \cos kl \end{pmatrix},$$

where  $l$  is the effective length of the quadrupole,  $k^2 = G/B\rho$  is the quadrupole strength, and  $B\rho$  is the magnetic rigidity (momentum per unit charge) of the particles in the assumed central trajectory. The matrix for the same quadrupole in the defocusing plane is

$$\mathbf{R}_d = \begin{pmatrix} \cosh kl & (1/k) \sinh kl \\ k \sinh kl & \cosh kl \end{pmatrix}.$$

If a beam monitor is placed a distance  $L$  downstream of a focusing quadrupole, then the matrix expressing the beam transformation from the entrance of the quadrupole to the monitor is given by the matrix product

$$\mathbf{R} = \mathbf{R}_L\mathbf{R}_f.$$

If the quadrupole gradient is varied, the size of the beam spot at the monitor will vary as described by eq. (4) with the transfer matrix just defined. Again the elements of the matrix  $\sigma^0$  are readily extracted from a set of profile measurements taken at several quadrupole settings.



The methods of this and the preceding section may easily be generalized to any set of  $\mathbf{R}$  matrices. It does not even have to be the same parameter, such as  $L$  or  $G$ , which is varied for each width measurement, as long as each transfer matrix connecting the points of measurement and the common point of origin is known in full.

### 3.3 Accuracy of the Method

Determination of the emittance at some point along the beam requires measurement of the three beam-matrix elements  $\sigma_{11}$ ,  $\sigma_{22}$ , and  $\sigma_{12}$ . When thinking about the accuracy of the emittance measurement it is useful to consider the beam at a waist, where  $\sigma_{12}^w = 0$ , and  $\epsilon = \sqrt{\sigma_{11}^w \sigma_{22}^w}$ . Three quantities describing the beam waist must be determined,  $\sigma_{11}^w$ ,  $\sigma_{22}^w$ , and  $z^w$ , the position of the waist. These are inferred from measurements of  $\sigma_{11}$  under various beam transport conditions as described above.

- The angular spread,  $\sqrt{\sigma_{22}^w}$ , of the beam can be found to high precision by simply comparing two beam profiles of sufficiently different size (due to an intervening drift or differing quadrupole focusing).
- The position of the waist,  $z^w$ , can be well determined from profile measurements that surround the waist (by a fit to the parabolic dependence of  $\sigma_{11}$  on  $z$ ).
- However, the beam size,  $\sqrt{\sigma_{11}^w}$ , at the waist can be well determined only by a profile measurement very near the waist itself. The extrapolation from other measurements determines  $z^w$  much better than the spot size at the waist.

Hence the uncertainty in the emittance is limited by the ratio of the detector spatial resolution to the size of the beam waist achievable at the monitor.

This argument is supported by detailed numerical simulation of the two methods for determining the emittance described above.

### 3.4 The “Pepper-Pot” Technique

When the entire beam is incident on a profile monitor, all information about the angular distribution is lost. However, if the beam is collimated into individual smaller ‘beamlets’ by apertures of known size, the divergence of these beamlets can be detected after they propagate a sufficient distance. Such a technique is called a ‘pepper-pot’ diagnostic and can yield simultaneous information about a beam profile and angular divergence in a single measurement. The pepper-pot technique is illustrated in Fig. 3.

The beam is screened upstream of the monitor by a “pepper-pot plate”, which contains a regular array of identical holes. Ideally the plate stops the beam, allowing only the beam incident on a hole to pass through to the profile monitor. The total intensity of each beamlet as a function of the position of the defining hole still provides a spatial profile of the beam. The profiles of individual beamlets can be used to extract information on the angular distribution of the beam at the position of the hole defining the beamlet.

The pepper-pot plate is shown in Fig. 3 as plane  $P$  and the beam monitor as plane  $M$  a distance  $L$  from the plate. The transverse spatial axes  $x$  and  $y$  are defined on  $P$  and a

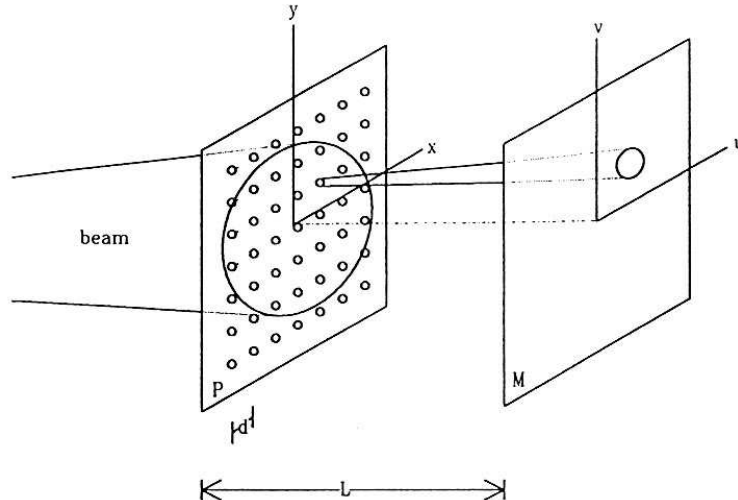


Figure 3: Concept of the “pepper-pot” method to measure transverse emittance.

parallel set of axes  $u$  and  $v$  on  $M$ . The origins of these coordinate systems are connected by a line parallel to the optic axis of the beam. A single collimated beamlet is shown. If a particle is known to pass through the point  $(x, y)$  on  $P$  and strike  $M$  at the point  $(u, v)$ , then the slopes of the particle’s path with respect to the optic axis are given by

$$x' = (u - x)/L,$$

$$y' = (v - y)/L.$$

Thus the beamlet spatial profiles in  $(u, v)$  are a direct measure of the angular distribution of the beam sampled at  $(x, y)$ .

From the pepper-pot image the emittance can be extracted in a straightforward manner if the beam is assumed to be Gaussian. However, one advantage of the pepper-pot diagnostic is that the shape of the beam in the  $x-x'$  and  $y-y'$  trace spaces can be determined explicitly and an *emittance plot* showing contours of constant beam intensity can be generated for each. Another advantage is that profile monitors designed to intercept the entire beam can also be used as part of a pepper-pot system simply by including a selection screen upstream. The pepper-pot plate shown in Fig. 1 is used in conjunction with the monitor shown downstream. When one of the schemes requiring the entire beam profile is employed, the plate can be withdrawn and the monitor used in that mode.

The precision of such a system is eventually limited by conflicting design considerations, and the necessary tradeoffs must be carefully optimized for a given application.

- The spatial distribution of the beam is best determined by sampling the beam at small spatial intervals, that is, by minimizing the hole spacing  $d$ , while the angular distribution is more precisely determined as the spatial profiles of the nonoverlapping beamlets get larger, maximizing  $d$ .

- Smaller holes allow more precise determination of a beamlet’s origin and minimize smearing of the angular profile due to variation of the angular distribution over the finite hole size, but smaller holes also sample a smaller fraction of the beam, decreasing the amount of signal.
- A plate thick enough to stop the beam or at least minimize the scattered beam (which contributes a diffuse background signal at the monitor) is desired, but the finite length of the holes (which may be much greater than their transverse size) may complicate the interpretation of beamlet profiles.

Estimates made for the ATF pepper-pot design indicate that the achievable precision is comparable to that estimated for the multiple-profile methods. It appears that the limiting accuracy of a transverse-emittance measurement is set by the resolution of the profile monitor, independent of the technique of extracting the emittance.

## 4 Longitudinal-Emittance Measurement

Monitors of the longitudinal emittance of a beam are less common than ones for the transverse emittance, but it is conceptually straightforward to map the longitudinal emittance onto an  $x$ - $y$  plane suitable for observation with a profile monitor. A dipole magnet that bends in the  $x$ - $z$  plane will disperse  $p_z$  onto  $x$ . A time-varying electromagnetic field can be made to deflect the beam in  $y$  by an amount dependent on  $t$ , which disperses particles with  $z = \beta ct$  onto  $y$ . With both effects occurring simultaneously, the  $z$ - $p_z$  density of the beam appears directly on the  $x$ - $y$  plane rather like the trace observed on an oscilloscope.

Dipole magnets of sufficient dispersive strength are readily available. Time-dependent fields of suitable strength and frequency can be found inside radio-frequency cavities. An interesting consequence of Maxwell’s equations is that no cavity operated in its lowest mode can impart a net transverse deflection to a relativistic particle. Hence deflection cavities must be operated in a higher mode, and a practical choice is the  $TM_{120}$  cavity described by Haimson [7] and sketched in Fig. 4.

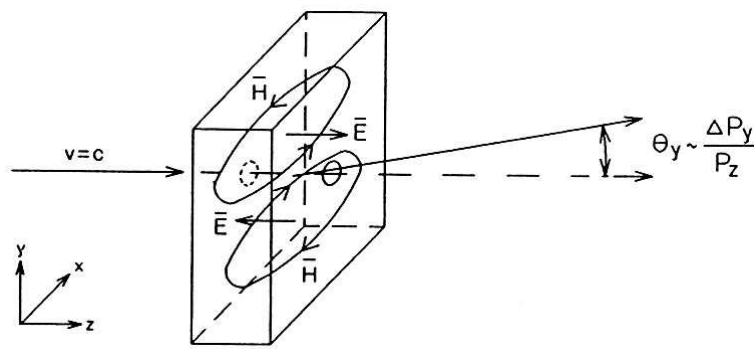


Figure 4: A  $TM_{120}$  rf cavity used to impart a time-dependent transverse deflection to a particle beam.

In the  $TM_{120}$  cavity the transverse deflection is caused by the magnetic field. Because the field is time varying, the deflection angle  $\theta_y$  depends on the time of arrival of the particle, conveniently measured as  $\Delta z$  relative to the center of a beam bunch. If the phase of the rf is adjusted so the center of the bunch suffers no deflection, then we may write

$$\theta_y = k\Delta z.$$

As seen in Fig. 4, the electric field  $E_z$  varies with  $y$  and will impart an acceleration or deceleration to the beam particles. This effect is unavoidable, and can be written

$$\frac{\Delta p_z}{p_z} = -ky,$$

with the same constant  $k$  as in the expression for  $\theta_y$ . A consequence is that the kicker will induce an undesirable spread in  $p_z$  if the beam is too large in  $y$ , ruining the momentum analysis of the beam by the dipole magnet. It may be necessary to trim the initial transverse emittance, perhaps by collimation in  $y$  before the beam enters the kicker. The way in which the kicker couples longitudinal to transverse phase space may be summarized by

$$\frac{\Delta z_i \Delta p_{z,f}}{p_z} = -y_i \theta_{y,f},$$

where  $i$  and  $f$  label quantities before and after the kicker, respectively.

It is important that the rf kicker be placed before the momentum-dispersing dipole, as the variation in path length through the dipole mixes  $\Delta z$ ,  $\Delta p_z$  and  $x$ . If this mixing occurred prior to the rf kicker the  $\Delta z$  analysis would not reflect the initial time distribution of the beam.

A facility for measuring the longitudinal emittance will be implemented in the beamline of the BNL Accelerator Test Facility, as sketched in Fig. 1. The rf kicker is placed just before the dispersing dipole D1. Dipole D2 is turned off, and the beam is brought to a focus on the profile monitor at the end of the ‘z-line.’ That is, a focus would be achieved when the kicker is off and the beam has zero momentum spread. A complication at the ATF is the requirement that the laser beam that triggers the photocathode of the electron gun must pass through the rf kicker. Hence the slit needed to collimate the beam in  $y$  cannot be placed next to the kicker as desired. Instead, quadrupoles Q4 and Q5 form an image of the kicker on the  $y$ -slit located between Q5 and Q9. It is anticipated that the profile of longitudinal emittance will have a time resolution of better than 1 picosecond and a momentum resolution better than 0.1%.

## 5 References

- [1] J. Liouville, *J. de Math.* **3** (1838) 349.
- [2] C. Lejeune and J. Aubert, *Emittance and Brightness: Definitions and Measurements*, in *Applied Charged Particle Optics*, Part A, A. Septier, ed. (Academic Press, New York, 1980), p. 159.

- [3] P. Lapostolle, CERN/DI-70-36 (1970).
- [4] X. Artru *et al.*, *Experimental investigations on geometrical resolution of optical transition radiation (OTR)*, Nucl. Instr. and Meth. A **410**, 148-158 (1998); *Resolution power of optical transition radiation: Theoretical considerations*, *ibid.* B **145**, 160-168 (1998).
- [5] P. Catravas *et al.*, *Beam Profile Measurement at 30 GeV Using Optical Transition Radiation*, Proc. PAC'99, pp. 2111-2113,  
<http://accelconf.web.cern.ch/accelconf/p99/PAPERS/WEA100.PDF>
- [6] K.L. Brown, *A First- and Second-Order Matrix Theory for the Design of Beam Transport Systems and Charged Particle Spectrometers*, SLAC-75 (June 1982).
- [7] J. Haimson, *Microwave and Beam Optics Design of Standing Wave Transverse Magnetic Deflection Systems*, Varian Associates Technical Memorandum TMO-90 (February 1966).